## Section 8

Development of and advances in ocean, sea-ice, and wave modelling and data assimilation.

# Impacts of Ocean Observing Systems in NCEP GODAS in the Tropical Pacific

Hyun-Chul Lee[1] and Daryl Kleist[2]
([1]IMSG at NOAA/NWS/NCEP/EMC, [2]NOAA/NWS/NCEP/EMC)
email : hyun-chul.lee@noaa.gov

The currently operational Global Ocean Data Assimilation System (GODAS, Behringer, 2007) assimilates in situ profile data from EXpendable BathyThermograph (XBT) and Conductivity Temperature Depth (CTD), stationary fixed moorings, autonomous Argo floats, and remotely sensed sea surface temperature. With GODAS, these ocean observing systems are fundamental to NCEP's operational efforts not only for monitoring the ocean state but also for forecasting multi-week to seasonal variability in the NCEP CFSv2. In order to evaluate the impact of the observation system on NCEP operational products, a series of observing system experiments (tOSE; Lee, et al. 2020) have been carried out, and the observational innovations and the analysis increments associated with individual ocean observations in NCEP's GODAS are monitored and evaluated.

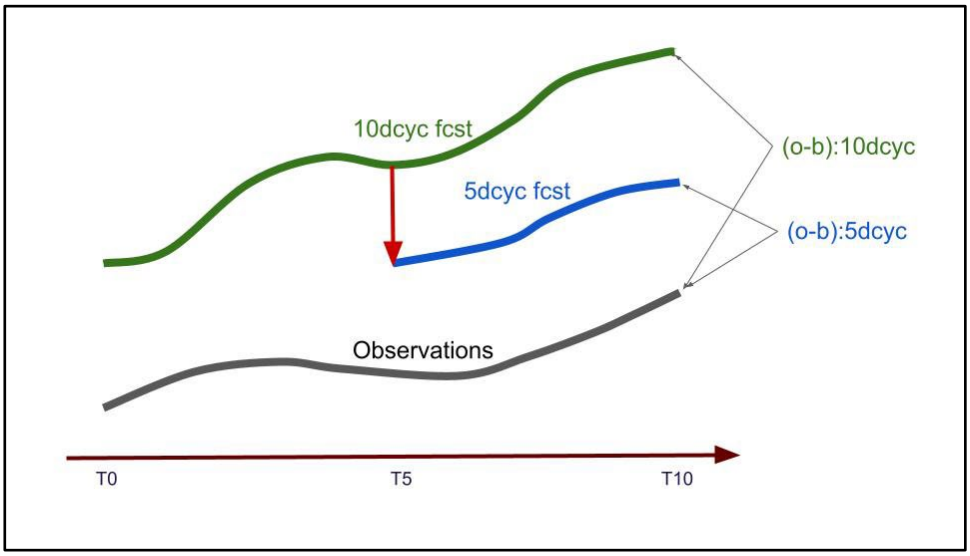


**Figure 1.** Schematic diagram showing trajectories of 10 day (green) and 5 day (blue) cycled runs, and real observations (black) in time. 10 day and 5 day cycled runs start at the same time, and the restart of 5day cycled runs from the analysis field (red arrow).

In the tOSE, the impacts of the observing systems on the GODAS are defined from the differences of absolute values of observation innovations between 5 day and 10 day cycle runs. Figure 1 shows a schematic diagram of the tOSE for 5 day/10 day cycle runs. At the end of the two runs, the differences are due to the updated initial states of the 5 day run. From the results of these differences, it is possible to estimate the impacts of each observing system on the GODAS, which is traceable at each observation in space and time.

In order to evaluate the impacts of the observing systems, the assimilation impacts of observing systems (AIOS) and the forecast impacts of observing systems (FIOS) are defined as

$$AIOS = \sum_{i=1}^{N} |o-b|_i \, , i \in regions \quad \text{and}$$

$$FIOS = AIOS_{10day} - AIOS_{5day}$$

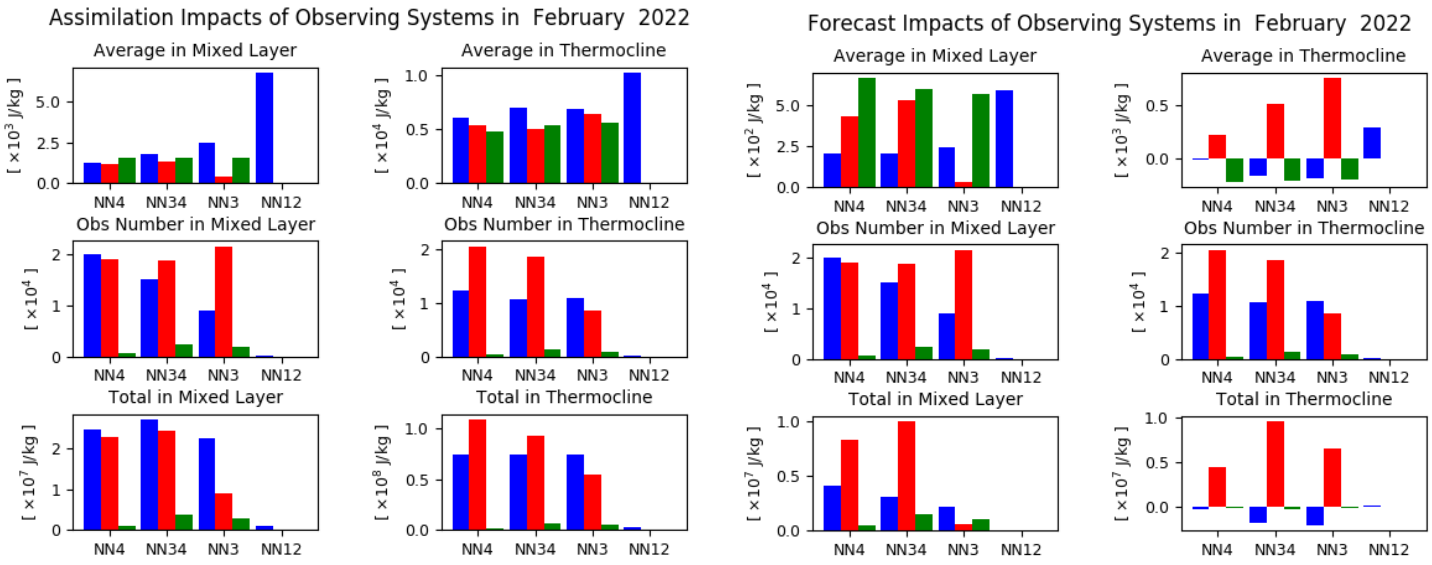


**Figure 2** Regional averaged AIOS (left) and FIOS (right) in February 2022 tropical Pacific oceans (right) from the observations of the Argo floats (blue), moored buoys (red) and CTD profiles (green), averaged over the NINO1+2 (NN12), NINO3 (NN3), NINO3.4 (NN34) and NINO4 (NN4) regions. Vertically, 'Mixed Layer' is the layer of temperature difference from SST that is less than 0.5ºC, and 'Thermocline' is the layer in the temperature range of 18 - 22ºC.

Figure 2 shows the energy-weighted AIOS and FIOS in February 2022, which are averaged in the regions of the tropical Pacific. During February 2022, the Argo (blue) and moored buoy (red) data are the main sources of in situ profile data in the tropical Pacific (middle row in Fig. 2). During this period, the relatively small amount of profile data from ships is also assimilated (green). The total AISO shows that the GODAS have been assimilated mainly from the Argo and moored buoy data. In the mixed layer, the profile data from Argo has larger impacts in the whole tropical Pacific. In the thermocline layer, the moored buoy data have larger impacts than Argo data. In February 2022, the Argo data induced more AIOS in the thermocline layer at NN3.

In the mixed layer, the FIOS of moored buoy data are two to three times larger than the FIOS from Argo in the NN4 and NN34 regions. In the thermocline layer, the moored buoy plays an essential role in FIOS for the whole tropical Pacific. The FIOS from Argo and ship data in the thermocline layer have the negative values. This means that actually FIOS in GODAS are degraded by these data in the regions in February 2022. This degradation of FIOS would be due to the dynamical mismatch between the real ocean and GODAS. The patterns and intensity of observational impacts in AIOS and FIOS change regionally and monthly, and the impacts of AIOS/FIOS in the NCEP GODAS have been monitored in near-real time. The tOSE's and monitoring systems of AIOS/FIOS are being developed for the application to the next version of GODAS.

**Acknowledgements**: This study was supported by NOAA's Global Ocean Monitoring and Observing Program.

**References:**

Behringer, D. W., 2007: The Global Ocean Data Assimilation System(GODAS) at NCEP. *Proc. 11th Symp. Integr. Obs. Assim. Systems*, San Antonio, TX, Amer. Meteor. Soc. 3.3.

Lee, H.-C., D. Behringer, D. Kleist, 2020, A traceable Observing System Experiment in NCEP GODAS, Research activities in Earth system modelling. Working Group on Numerical Experimentation. Report No. 50. WCRP Report No.6/2020. WMO, Geneva (http://bluebook.meteoinfo.ru/index.php?year=2020&ch_=2), pp.1-11--1-12.

# Modeling of the Caspian Sea ice on a seasonal scale

E.S.Nesterov, V.D.Zhupanov, A.V.Fedorenko
*Hydrometeorological Research Centre of Russian Federation*
*Email: nesterov@mecom.ru*

## Introduction

The ice cover of the Caspian Sea, which is formed mainly in its northern part from November to March, has a significant impact on shipping, oil and gas production. The methods used to predict the characteristics of the Caspian Sea ice are usually based on statistical relationships between meteorological and ice parameters. As an example, there is a method of short-term forecasting of ice thickness in the northeastern part of the Caspian Sea, based on the relationship between the sum of negative air temperatures in forecast for 3-5 days and the ice thickness increase (Naurozbayeva, Lobanov, 2020).

Recently, hydrodynamic models have been used to predict the characteristics of ice conditions. The paper (Fomin et al. 2020) presents the results of a 24-h forecast of ice conditions in February 2017. Our paper discusses the results of experimental application of the **C**ommunity **I**ce **C**od**E** (CICE) model for modeling the ice characteristics of the Caspian Sea in the winter seasons of 2005-2008.

## Model configuration and data used

Most of the sea ice parametrization and modeling systems developed in recent years have been assembled by the scientific community and integrated into complex sea ice models. The most advanced and complete of them, apparently, is the CICE sea ice model (CICE Documentation, 2021). The general access software of the CICE model is distributed in combination with the Icepack package, the set of physical parameters of which takes into account thermodynamic and dynamic subgrid processes. To account for changes in the sea ice thickness, the ice cover is divided into several classes in the CICE model. Each class represents a range of sea ice thickness and describes the evolution of the thickness distribution in time and space. The CICE model is used at several prognostic centers.

To simulate the characteristics of the Northern Caspian Sea ice based on the CICE-v6 package 6.3 (CICE Documentation, 2021), a version of an autonomous forecast model with a bi-polar orthogonal computational grid (Bouillon et al.,2009; Ross, 1996) and anisotropic elastic-viscous-plastic rheology (Hunke et al.,2011) has been created. This approach makes it possible to perform numerical experiments using the extensive test archive of the CICE consortium, which includes the following global data:

- seabed bathymetry;
- monthly average water temperature, salinity and currents;
- 3-hour reanalysis data of JRA55 (Tsujino et al.,2018) from 2005 to 2009 for short-wave and long-wave radiation fluxes, wind direction and speed, air temperature and humidity.

## Results of modeling the ice characteristics for the Caspian Sea

Ice characteristics were calculated for four winter (October-March) seasons of 2005-2009. The numerical results were analyzed for the area near Bolshoy Peshnoy Island, as it is most representative for the ice conditions of the Northern Caspian Sea (Naurozbayeva, Lobanov 2020). The ice concentration and thickness were calculated along with the dates of ice formation and disappearance. The quality of modeling was evaluated by comparing the calculated and actual dates of ice formation and disappearance, as well as the maximum ice thickness and the dates of its formation.

The dates of ice formation and disappearance were determined by calculation of ice concentration. In three cases (2005, 2006 and 2008), the calculated ice formation dates were nearly correct (the error was 1 - 4 days). In all cases, the ice actually disappeared earlier than in calculations (by 4 days in 2006 and 24 days in 2008). The greatest differences in the maximum thickness and the date of formation relate to January-March 2007, when the ice thickness was the

smallest of the four seasons (15 cm). At the same time, in February 2008, when the thickness was the largest (60 cm), the calculation can be considered satisfactory, both in thickness (47 cm) and in the date of formation (see Figure).

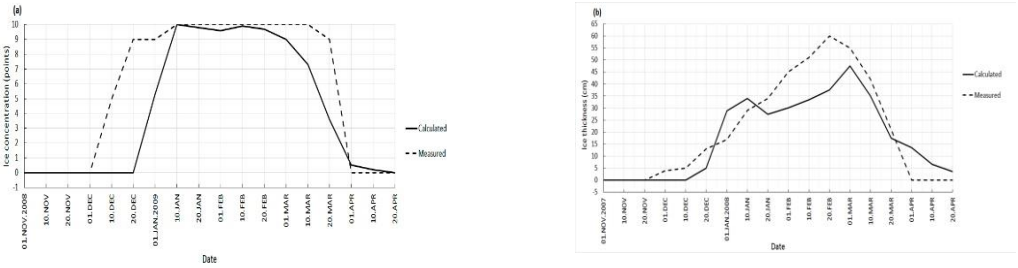


Fig. Calculated and measured ice concentration (points) in the winter season 2008-2009 (a) and ice thickness (cm) in the winter season 2007-2008 (b).

**Conclusions**

Based on numerical experiments with the CICE model (version V6.3) it is shown that the CICE model with a bi-polar orthogonal computational grid and anisotropic elastic-viscous-plastic rheology satisfactorily reproduces the processes of ice build-up and melting in the Caspian Sea. In some years there are significant discrepancies between the calculated and actual dates of ice formation and disappearance. It should be noted that the results of calculating the ice maximum thickness coincide well with the observational data.

**References**

Bouillon S. et al. An elastic–viscous–plastic sea ice model formulated on Arakawa B and C grids //Ocean Modelling. 2009.Vol. 27.No.3-4. P. 174-184.

CICE Documentation 2021, https://github.com/CICE-Consortium/

Fomin V.V., Diansky N.A., Korshenko E.A., Vyrachalkina T.Y. System of operative diagnosis and forecast of hydrometeorological characteristics of the Caspian Sea and assessment of the accuracy of forecasts based on field measurements // Meteorology and hydrology. 2020. No. 9. pp. 49-64.

Hunke E. C. et al. The multiphase physics of sea ice //Sea. 2011.Vol. 5. P.1949-1993

Hebert D. A., Allard R. A., Metzger E. J, Posey P. G. et al. Short-term sea ice forecasting: an assessment of ice concentration and ice drift forecasts using the U.S. Navy's Arctic Cap Nowcast/Forecast System// J. Geophys. Res. Oceans.2015. Vol. 120. P. 8327–8345. doi:10.1002/ 2015JC011283

Naurozbayeva Zh.K., Lobanov V.A. Methodology of short-term forecasting of ice thickness increase in the north-eastern sector of the Caspian Sea// Geographical Bulletin. 2020. No. 3(54). pp. 81-97.

Rae J. G. L.., Hewitt H. T., Keen A. B., Ridley J. K. et al. Development of the Global Sea Ice 6.0 CICE configuration for the Met Office Global Goupled model// Geosci. Model Dev. 2015.Vol. 8. P.2221–2230

Ross J. M. Explicit Generation of Orthogonal Grids for Ocean Models// J. Computational Physics. 1996. Vol.126. P. 251–273.

Tsujino H. et al. JRA-55 based surface dataset for driving ocean–sea-ice models (JRA55-do) //Ocean Modelling. 2018. Vol. 130. P. 79-139

# Real-Time Extension of NOAA-NCEP Next Generation Global Ocean Data Assimilation System (NG-GODAS)

Shastri Paturi[1], Jieshun Zhu[2], Travis Sluka[3], Guillaume Vernieres[4], Andre van der Westhuysen[1], Daryl Kleist[4]

[1]IMSG@NOAA/NCEP/EMC, [2]NOAA/NCEP/CPC, [3]JCSDA, [4]NOAA/NCEP/EMC
Email: Shastri.Paturi@noaa.gov

As part of the collaborative development effort for the Unified Forecast System (UFS) Research-to-Operations (R2O) Project, a 40-year reanalysis was completed for the period of January 1979 – August 2019. This reanalysis was based on the NG-GODAS system, where the ocean model has a 1-deg horizontal resolution and 75 layers in the vertical. The model set-up, resolution, forcing, data assimilation scheme and ingested observations are described in [1]. To better serve the ocean monitoring task at the National Oceanic and Atmospheric Administration (NOAA), the National Centers for Environmental Prediction/Environmental Modeling Center (NCEP/EMC) and NCEP/CPC (Climate Prediction Center) are working together to set up the NG-GODAS in a real-time configuration to replace a 20-year old operational ocean data assimilation system (GODAS). As a first step of this joint effort, the NG-GODAS run is being extended from September 2019 up to real-time, and is initialized from the ocean and sea-ice state from the 40-year reanalysis.

For the real-time extension of the NG-GODAS, changes had to be made to the atmospheric forcing and some ingested observations because of their unavailability in real time.

Atmospheric forcing: the Global Ensemble Forecast System (GEFS) forcing, obtained from NOAA/PSL (Physical Sciences Laboratory) used in the later period of the 40-year reanalysis is not available after 2019. For the real-time extension run, the CFSR forcing with a bias correction [2] is applied for the period of January 2020 - March 2021 and the Global Data Assimilation System (GDAS) forcing is used after that.

In-situ observations: Temperature and salinity profiles from the US Navy's Fleet Numerical Meteorology and Oceanography Center (FNMOC) are assimilated. These data are passed through the Navy Coupled Ocean Data Assimilation's (NCODA) Quality Control System (QC) [3].

SST: Level 4 SSTs from the Operational Sea Surface Temperature and Sea Ice Analysis (OSTIA) analysis are assimilated, which are produced daily on an operational basis at the UK Met Office using optimal interpolation (OI) on a global 0.054° x 0.054° degree horizontal resolution (https://resources.marine.copernicus.eu/product-detail/SST_GLO_SST_L4_NRT_OBSERVATIONS_010_001/). The data are superobbed onto the 1° model grid with the number of observations being assimilated reduced from 17 million to 80000. The superobbing process increases the error estimates based on the variance of the original data within each bins (Figure 1).

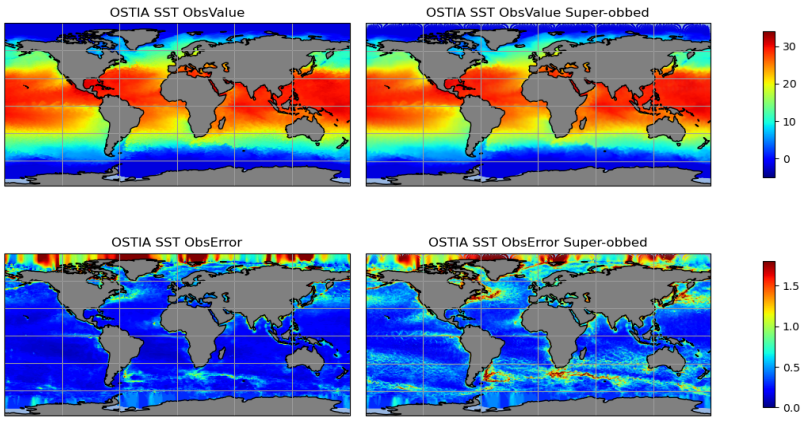


Figure 1. Superobbed OSTIA L4 SST data for August 31, 2019.

Sea-ice concentration: Level 4 sea ice fractions of the Climate Data Record (CDR) are assimilated, which are produced by the National Snow & Ice Data Center (NSIDC) from passive microwave on a 25km x 25km grid for the Northern and Southern Hemispheres (ftp://sidads.colorado.edu/pub/DATASETS/NOAA/G02202_V4).

The current version of the data atmosphere option of the UFS coupled global atmosphere sea ice (DATM-MOM6-CICE6; [1]) model being cycled with JEDI-SOCA [1] data assimilation is based on the prototype P7c. The model

has been integrated from 2019-08-31 to 2019-12-31 with GEFS forcing, and with CFSR forcing for the period 2020-01-01 to 2021-03-31. The model temperature and salinity are compared with two current operational ocean data assimilation systems at NOAA (CFSR and GODAS) by validating against the UK Met Office Hadley Center EN4.2 objective analysis [4]. Figure 2 shows the mean difference of GODAS, CFSR and NG-GODAS compared against EN4 for the period of simulation in the top 300m. The results show that there is significant improvement over both GODAS and CFSR in the salinity field with the NG-GODAS system, whereas the temperature field is comparable with both GODAS and CFSR. The current configuration will be run in real-time mode as an operational system by NCEP/CPC.

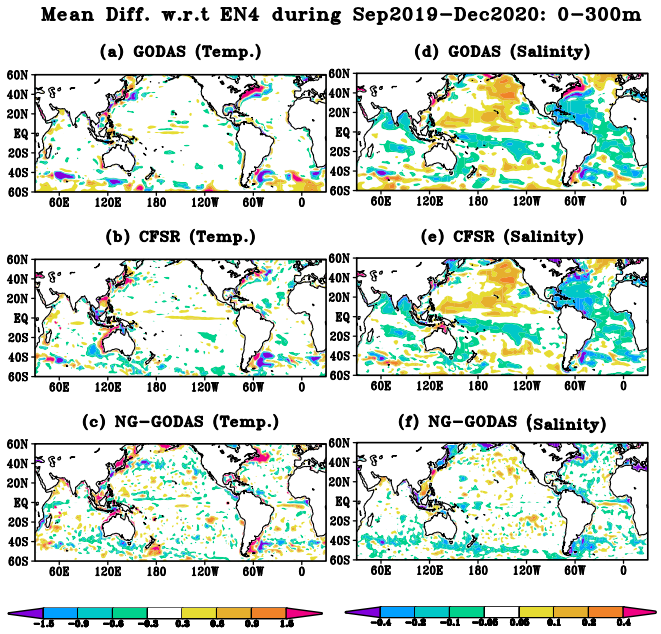


Figure 2. Mean difference of upper 300m averaged (left) temperature and (right) salinity in GODAS, CFSR and NG-GODAS relative to EN4 for the period 2019-09 till 2020-12.


[1] The NOAA-NCEP 40 year reanalysis with the Next Generation global Ocean Data Assimilation System (NG-GODAS): 1979-2019, U.S. D.O.C, NOAA, NWS, NCEP Tech Note not yet published)

[2] J.Kim, Y.C.Teng, G.Vernieres, T.Sluka, S.Paturi, Y.Hao, D.Worthen, B.Li, J.Wang, J.S.Zhu, H.C.Kim, D.Kleist. "NOAA-NCEP Next Generation Global Ocean Data Assimilation System (NG-GODAS)." Research activities in Earth system modelling. Working Group on Numerical Experimentation. Report No. 51. WCRP Report No.4/2021. WMO, Geneva (http://bluebook.meteoinfo.ru/index.php?year=2021&ch_=2), pp. 8-05—8-06.

[3] www.usgodae.org/pub/outgoing/fnmoc/data/ocn/.

[4] S.A. Good, M.J. Martin and N.A.Rayner, 2013: EN4: Quality Controlled ocean temperature and salinity profiles and monthly objective analyses with uncertainty estimates. Journal of Geophysical Research, 118.6704-6716.

# Evaluation of Ocean and Sea-ice Model States in a 20-year Spin-up of 1/4deg UFS DATM-MOM6-CICE6 and HYCOM-CICE4 Models

Shastri Paturi[1], Alexandra Bozec[2], Eric Chassignet[2], Andre van der Westhuysen[1], Daryl Kleist[3]

[1]IMSG@NOAA/NCEP/EMC, [2]COAPS/FSU, [3]NOAA/NCEP/EMC

Email: Shastri.Paturi@noaa.gov

## 1. Introduction

NOAA/NCEP develops and runs operational ocean forecasting models at various horizontal resolutions (0.5 deg: CFSR; 1deg GODAS; 1/12 RTOFS-v2). The Unified Forecast System (UFS) being developed at NOAA aims to provide forecasts at seasonal to sub-seasonal (S2S) scales at 0.25 deg resolution. The purpose of this work is to evaluate the response of two ocean sea-ice coupled models to the same atmospheric forcing initialized from a state of rest.

To achieve that aim, several metrics, including model drifts, surface biases, sea-ice extent and volume will be used. This first step will then help quantify the impact of data assimilation. This paper describes the model setup and preliminary results.

## 2. Method

The ocean sea-ice coupled models, UFS DATM-MOM-CICE6 [1] and HYCOM-CICE4 [2], are set-up at 0.25 deg horizontal resolution based on the MOM6 grid with 41 vertical layers based on the HYCOM vertical grid. Both the models are initialized with the temperature and salinity profile from the World Ocean Atlas (WOA) 2018 climatological dataset and with surface forcing (air temperature, precipitation, etc.,) from the global ensemble forecast system (GEFS), for the period 2000-2019. For sea-ice concentration and thickness, the default initialization values from the CICE6 and CICE4 model were used. The model parameters are kept as close as possible in the two models.

## 3. Results

The average modeled and climatological (WOA18) sea surface temperature (SST) and sea surface salinity (SSS) are calculated for two periods: 2000-2005 and 2010-2019. The modeled SST and SSS bias are estimated from the difference between the two models and WOA18. Figures 1 and 2 show that the SST from the UFS DATM-MOM6-CICE6 is colder than the WOA18 climatology in the tropical open ocean while the HYCOM-CICE 4 SST is warmer for both periods compared. An increase in the cold bias in both models is seen for the period 2010-2019 (Figure 2).

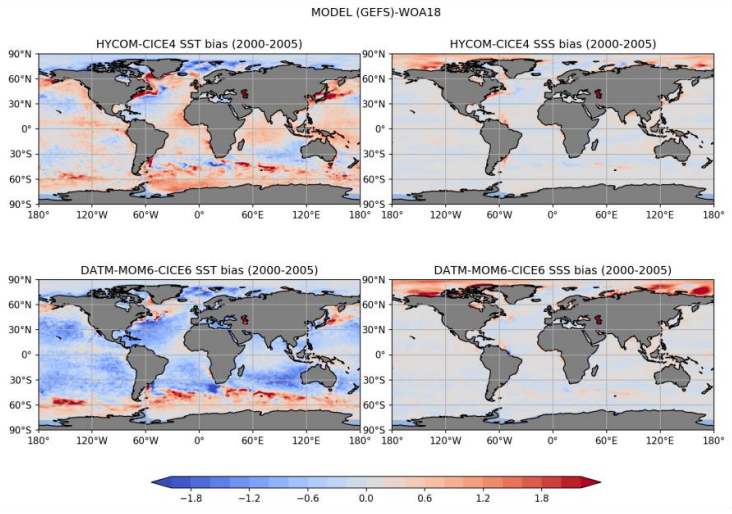


**Figure 1** Bias of modeled (DATM-MOM6-CICE6 and HYCOM-CICE4) SST and SSS from WOA18 for the period 2000-2005.

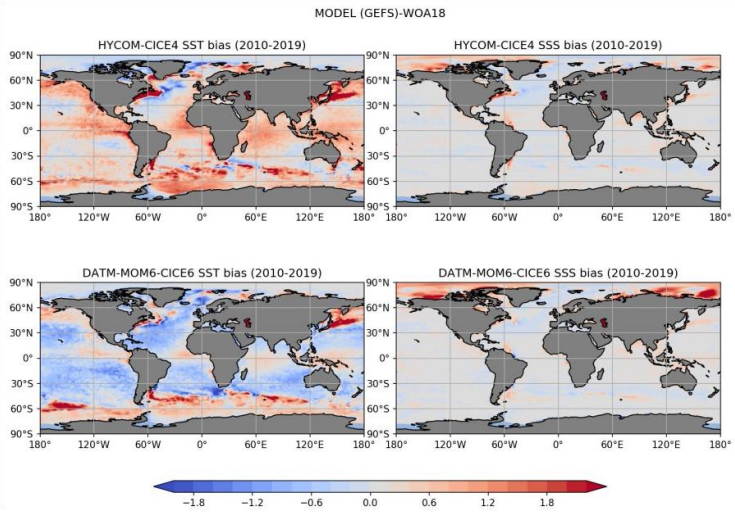


**Figure 2** Bias of modeled (DATM-MOM6-CICE6 and HYCOM-CICE4) SST and SSS from WOA18 for the period 2010-2019.

The time-series of sea-ice extent (SIE), defined as the region covered with sea-ice with a threshold of 15% sea-ice concentration, and the total ice volume between the two models are shown in Figures 3 and 4 for the Arctic and the Antarctic. The total sea-ice volume from the two models is also compared against the Pan-Arctic Ice-Ocean Modeling and Assimilation System (PIOMAS) total ice volume. Figure 3 shows a reasonable comparison of the total sea-ice volume from the two models compared with PIOMAS. However, in the Antarctic the SIE and total sea-ice volume is larger in the DATM-MOM6-CICE6 than in HYCOM-CICE4.

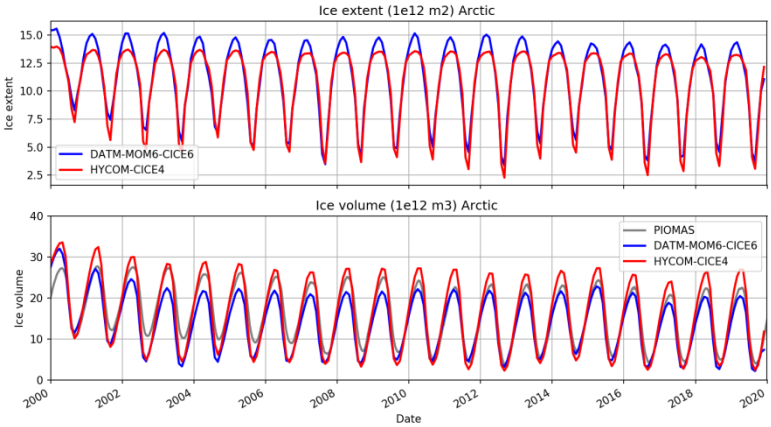


**Figure 3** Sea-ice extent and total sea-ice volume for the period 2000-2019 in the Arctic between DATM-MOM6-CICE6 and HYCOM-CICE4. The total sea-ice volume is compared against PIOMAS[3].

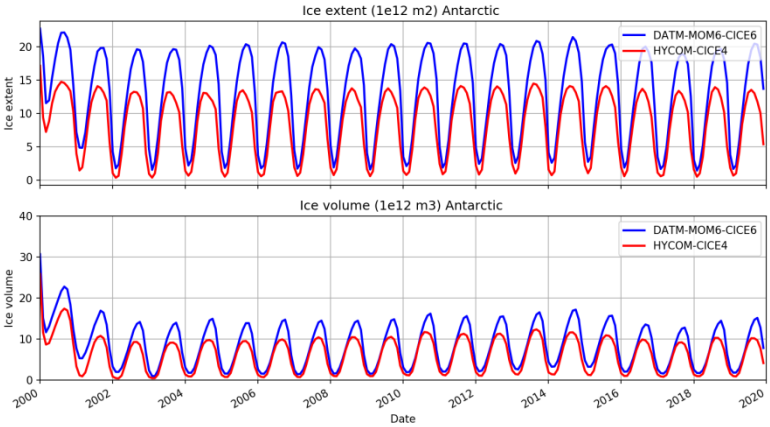


**Figure 4** Sea-ice extent and total sea-ice volume for the period 2000-2019 in the Antarctic between DATM-MOM6-CICE6 and HYCOM-CICE4.

## References


[1] J.Kim, Y.C.Teng, G.Vernieres, T.Sluka, S.Paturi, Y.Hao, D.Worthen, B.Li, J.Wang, J.S.Zhu, H.C.Kim, D.Kleist. "NOAA-NCEP Next Generation Global Ocean Data Assimilation System (NG-GODAS)." Research activities in Earth system modelling. Working Group on Numerical Experimentation. Report No. 51. WCRP Report No.4/2021. WMO, Geneva (http://bluebook.meteoinfo.ru/index.php?year=2021&ch_=2), pp.8-05--8-06.

[2] J.Cummings, Z.Garraffo, D.Iredell, S.Paturi, Y.Hao, T.Spindler, B.Alasubramanian, A.Mehra. "Ocean Data Impacts in the Real Time Ocean Forecast System: RTOFS-v2." Research activities in Earth system modelling. Working Group on Numerical Experimentation. Report No. 51. WCRP Report No.4/2021. WMO, Geneva (http://bluebook.meteoinfo.ru/index.php?year=2021&ch_=2), pp.8-03—8-04.

[3] Schweiger, A., R. Lindsay, J. Zhang, M. Steele, H. Stern, Uncertainty in modeled arctic sea ice volume, J. Geophys. Res., doi:10.1029/2011JC007084, 2011.

# Effect of Higher Resolution and Advanced Atmospheric Physics Package on Week 3&4 Equatorial Thermocline Forecasts

Sulagna Ray[1], Lydia Stefanova[2], Jiande Wang[2], Jessica Meixner[3], and Avichal Mehra[3]
[1]SRG at NOAA/NCEP/EMC, College Park, Maryland, US
[2]IMSG at NOAA/NCEP/EMC, College Park, Maryland, US
[3]NOAA/NCEP/EMC, College Park, Maryland, US
Email: sulagna.ray@noaa.gov

## 1. Introduction

In recent configurations, NCEP/EMC Unified Forecast System (UFS) coupled prototypes for subseasonal to seasonal forecasts introduced an advanced atmospheric physics package and increased the atmospheric resolution from L64 to L128. This affects forecasts of upper and lower level winds which in turn influences the upper ocean in regions of strong ocean-atmosphere coupled interaction, in particular the equatorial oceans. The zonal slope and depth of equatorial thermocline (D20) changes if (i) there is a net increase/decrease in heat uptake by the ocean, (ii) a strengthening/weakening of equatorial zonal wind stress ($\tau_x$), and/or (iii) changes in near-equatorial wind stress curl that enhances/diminishes the equatorial Ekman upwelling and poleward Sverdrup transport. In this study we validate the changes in week 3&4 forecasts of D20 between coupled UFS Prototype 5 (P5) and Prototype 6 (P6) (Stefanova et al., 2022), and quantify processes that could drive the changes. The atmospheric components of P5 and P6 use the FV3 dynamical core, but the physics package and vertical levels in P5 (GFSv15.2, L64) are updated in P6 (GFSv16, L128). GFSv16 includes updates in PBL/turbulence scheme, the solar radiation absorption by water clouds, the microphysics scheme for computing ice cloud effective radius, and added parameterization of subgrid scale nonstationary gravity wave drag. The ocean (MOM6), ice (CICE6) and wave (WAVEWATCH III) components remain unchanged between P5 and P6. In the following section we present results of forecasts of week 3&4 average, for the period April, 2011-March, 2018. Although the wind stress from ERA5, and radiation flux from CERES-flux are daily fields for validation, D20 from ECMWF-ORAS5 is monthly. Thus, the bias in standard deviation ($\sigma$) in D20 is subject to a minimal error on comparing a bimonthly to a monthly time series.

## 2. Results

### *Pacific Ocean*

Strong easterly $\tau_x$ with a larger $\sigma$ in the west and a strong east-west sloping D20 with its largest $\sigma$ in the east remain unchanged in P6 (Fig 1, 2). In general, a deepening of D20 in P6 is associated with a decrease in easterlies, but a negative heat uptake from P5→ P6 into the ocean. The systematic underestimation of $\tau_x$ variability around the dateline, especially in OND – the season of strong winds – indicates a deficiency in capturing the intra-seasonal wind variations (particularly related to ENSO anomalies). This under-represents the D20 variability (in OND) between 150°W-120°W, in spite of having minimal depth bias (Fig 1). Seasonally, the mean $\tau_x$ bias varies between the prototypes, with P5 showing less bias in OND, and P6 in MJJ - indicating seasonally dependent improvement in $\tau_x$. Weakening of mean equatorial easterlies in P6 in OND do not drive changes in D20 entirely. Instead further eastward an enhanced shallow bias (Fig 1) is likely associated with strengthening of off-equatorial wind stress curl (for December ICs only), which strengthens the Ekman upwelling and shoals the equatorial D20 in P6.

### *Indian Ocean (IO)*

The mean slope of equatorial D20 is flatter compared to the Pacific, and is dominated by westerly $\tau_x$. Seasonally, P6 captures better the strengthened westerlies in OND, and the zonal $\tau_x$ pattern in MJJ. An increase in $\tau_x$ strength and an improved $\sigma$ (particularly in the east in MJJ, and west in OND) reduces the $\tau_x$ bias P6. This likely drives the overall decrease in D20 bias, particularly in the east, in absence of any increase in radiative heating of the ocean. The small $\sigma$ in D20 is similar to ORAS5 and remains almost unchanged in P6. However, the shallow D20 bias in the east is largely reduced in P6 (mostly in MJJ). A possible mechanism could be the strengthening of low level westerlies and upper level easterlies from P5 → P6, which strengthens the Walker circulation. Although that improves the D20 in the east, it does little to change the bias in the west, which requires further investigations.

### *Atlantic Ocean*

The D20 variability is too large and $\tau_x$ variability is too weak in both P5 and P6. The seasonal strengthening of easterlies (particularly in MJJ) is also not captured. Although the mean $\tau_x$ bias decreases in the east and increases in the west in P6, it does not seem to drive the mean bias in D20, which deepens basinwide in P6. Instead, an increase in net radiative heat uptake by the ocean seems consistent with D20 deepening in P6.

## 3. Summary

In summary, we find regionally and seasonally dependent improvements in equatorial D20 forecasts in P6. Although the bias improves slightly in the central equatorial Pacific, it increases in the eastern equatorial regions. In IO, the bias is reduced in the east, with no clear improvement in the west. In the Atlantic, however, the forecast remains unchanged, except for a deeper D20 in the west. In both the IO and Pacific changes in bias are related to changes in $\tau_x$ and wind stress curl bias, however, changes in net radiative heat uptake seem to dominate the Atlantic.

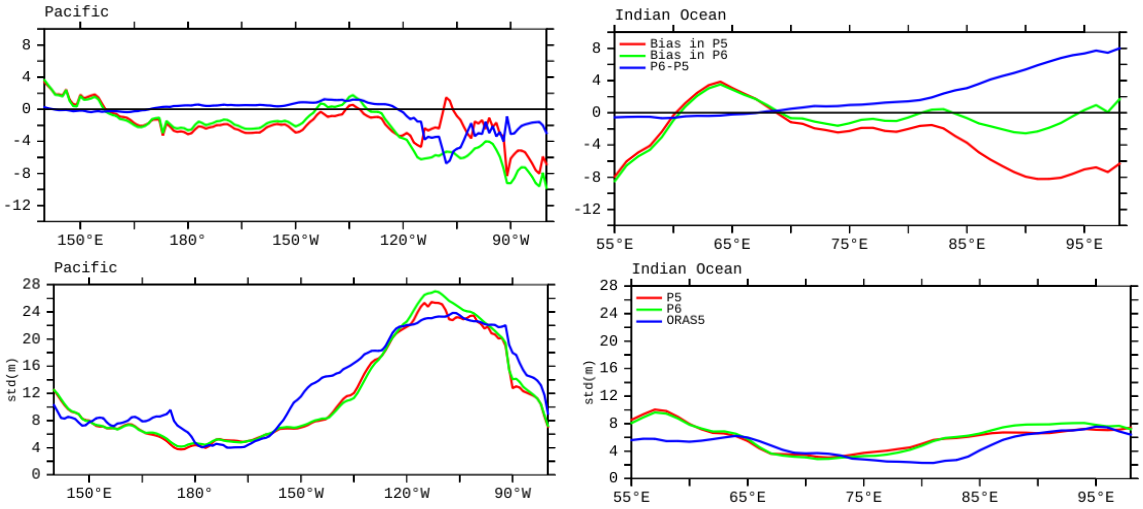


**Fig 1.** Mean week 3&4 forecast bias in equatorial (2°S-2°N) D20 (top) and σ (bottom) for OND in the Pacific (left) Indian Ocean (right). Bias assessed with ORAS5. Legends provide description of the colored lines.

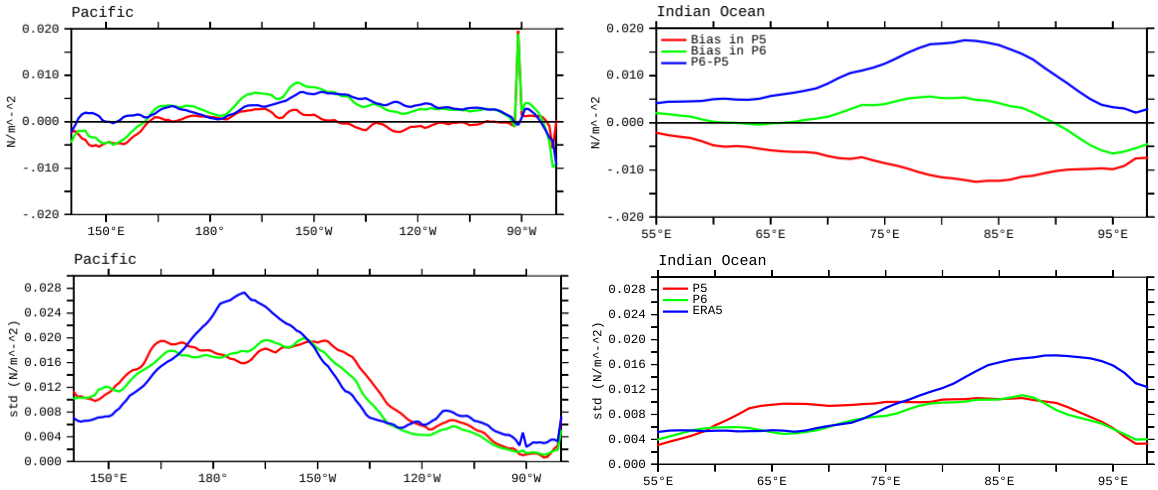


**Fig 2.** As in Fig 1 but for $\tau_x$. Bias assessed with ERA5.

## References

Stefanova, L., et al., 2022: Description and Results from UFS-Coupled Prototypes for future Global, Ensemble and Seasonal Forecasts at NCEP, NCEP Office Notes (In preparation).

# Influence of Short-Period Variations of Atmospheric Forcing on Large-Scale Ocean Dynamics

Yu.D. Resnyanskii, A.A. Zelenko, V.N. Stepanov, and B.S. Strukov
*Hydrometeorological Research Center of Russian Federation*
*Email: resny@mail.ru*

## Introduction

The variability of the ocean dynamics is controlled by both atmospheric forcings (AF) on its surface and its own internal dynamics. Due to the nonlinearity, dynamical processes in the ocean at different time scales interact with each other. Consequently, the structure and evolution of oceanographic fields, even at larger scales, also depend on the short-period variability of the AF, no matter how short.

Estimates of this dependence are obtained using the ocean general circulation model, which is part of the oceanographic data assimilation system of the Hydrometeorological Center of Russia.

## Numerical experiments

These estimates were obtained by comparing the results of two numerical experiments carried out over the period 2001–2014 with atmospheric forcing DFS5.2 (DRAKKAR Forcing Sets, Dussin et al., 2016). The simulations started from initial state of rest with the January climatological temperatures and salinities from the WOA13 atlas. The experiments differed only in the time discreteness of the AF sets (air temperature and humidity at a height of 2 m, wind speed at a height of 10 m, downward fluxes of short-wave and long-wave radiations, and precipitation rate): 3–24 hours in the main experiment (further as E1 experiment) and 1 month in the experiment with the time- averaged AF (E2).

The ORCA1 configuration of the NEMO version 3.6 model (Madec, 2008) coupled to the LIM3 ice model (Rousset et al., 2015) was used for the numerical experiments. All model outputs in both experiments were stored as successive 5-day means throughout the whole integration period.

## Results

### *Kinetic energy*

The kinetic energy averaged over the World Ocean within the entire water column from the surface to the bottom, normalized to the density of water $KE = \overline{\frac{1}{2}(u^2 + v^2)}$ ($u$ and $v$ are the 5-day averages of the horizontal velocity components, the overbar denotes averaging over area and depth) in the E1 experiment was systematically higher by ~20% compared to E2. By the end of the fourth model year, a quasi-steady state has been reached with KE fluctuating between 5(4) and 6.5(5) $cm^2s^{-2}$ for the E1 (E2) experiment that indicates a fast baroclinic adjustment of the velocity field to the initial density field, which subsequently has been slowly changed.

### *Atlantic meridional overturning circulation and meridional heat transport*

The upper cell of the Atlantic meridional overturning circulation (AMOC) in almost the entire Atlantic in E1 turned out to be more intense than in E2, with maximum differences between E1 and E2 to the south of 20°N about of 2–5 Sv (1 Sv = $10^6 m^3/s$). Near-surface circulation cell driven by wind between 30°N and 60°N, in E1 it also turned out to be ~2 Sv more intense than in E2. The Deacon cell in E2 is about 15 Sv weaker than in E1.

The elimination of short-term variability of the AF led to a decrease in meridional heat transport (MHT) in the Atlantic Ocean from 35°S up to ~30°N by almost 30%. This decrease is mainly due to the weakening of the AMOC. The MHT weakened by ~15–20% to the north of 45°N due to a decrease of the contribution of the oceanic circulation gyre to E2. The exception is the region from ~37°N up to ~45°N (at the boundary of oceanic gyres), where the MHT value from E2 exceeded the value from E1, and the difference between the MHT values at ~40°N reached almost 40%.

### *Thermohaline fields*

One of the most distinct consequences of the impact of short-period variations, noted in (Resnyanskii and Zelenko, 1999), is a change of the seasonal cycle of the surface water temperature. In our experiments, a decrease in the seasonal changes of the surface temperature due to short period variations was noted, as is seen from the map of amplitude differences between E1 and E2 (Fig. 1a). It was the most noticeable in moderate and high latitudes polewards of 40°N and 40°S. The magnitude of the decrease (~2°C) was almost quarter of the amplitude of seasonal cycle itself (~8°C). The reverse picture was observed in the subtropical latitudes ($|\varphi|$ = 20–40°) where the amplitude increased. The influence of the short-term AF variations on

seasonal changes in near-surface salinity in most areas was either weak or almost independent of the AF type (Fig. 1b).

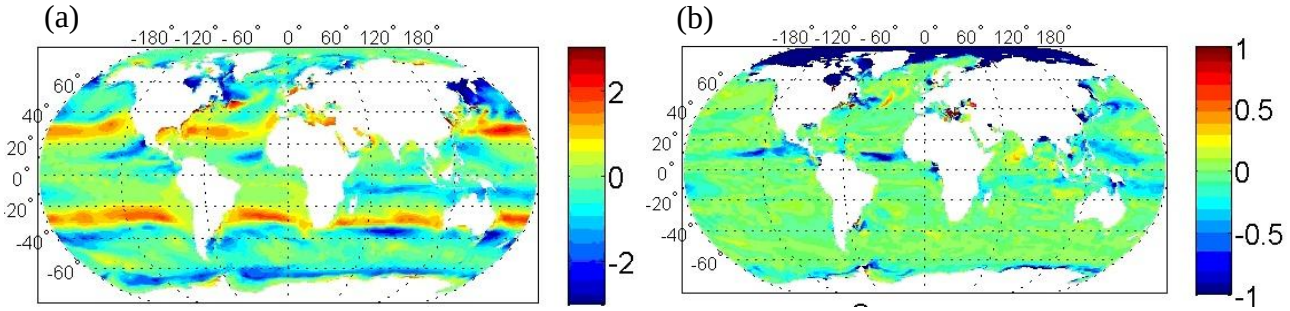


Fig. 1. Difference between amplitudes of seasonal changes in surface temperature (a) and salinity (b) in experiments E1 and E2. The amplitude is defined as 2009–2013 mean module of the difference between monthly averages in September and March.

From a comparison of the modelled temperature fields with the WOA13 data, the results of calculations in E1 are in better agreement with WOA13 than E2. Due to the stronger Ekman pumping in E1, the salinity in the area of subtropical ocean gyres turns out to be higher. The salinity field is slightly better reproduced in E2 up to ~45°N, however, to the north of 45°N, the model salinity field in E1 is closer to the observational data. Thus, considering the short-term variability of the AF allows to more accurately reproduce the temperature field in all areas of the World Ocean and the salinity field at high latitudes.

***Sea Ice***

In seasonal changes of the area occupied by sea ice, a significant difference between E1 and E2 in the Northern hemisphere was observed from June to September: the area occupied by sea ice in E2 exceeded the NOAA/NSIDC observed value in August, while in E1 this area was underestimated in August by about by $2\times10^6$ km$^2$. Both calculations overestimate the area occupied by sea ice, but the difference between the calculation results of E1 and the NOAA/NSIDC data was two times less than for E2.

A closer agreement between the results of the E1 experiment and NOAA/NSIDC data is also noted for calculations for the seasonal variability of sea ice volume. In the northern hemisphere, the monthly averaged volume of sea ice in E1/E2 ($14.3\times10^3$/$15.3\times10^3$ km$^3$) varies from a minimum of $4.1\times10^3$/$7.8\times10^3$ km$^3$ in August-September to a maximum of $25.1\times10^3$/$22.9\times10^3$ km$^3$ in April (according to PIOMAS data minimal and maximal values are $4.2\times10^3$ and $22.3\times10^3$ km$^3$, respectively). In the southern hemisphere, the monthly averaged volume of sea ice in E1/E2 reaches its maximum in October $18.9\times10^3$/$17.5\times10^3$ km$^3$ and then decreases to $2.7\times10^3$/$5.2\times10^3$ км$^3$ in February (according to GIOMAS data, the maximum value in September–October is $18.7\times10^3$ km$^3$, and minimum in February is $1.9\times10^3$ km$^3$).

**Summary**

The results of numerical experiments with the ORCA1/LIM3 model indicate that neglecting short-term variations in atmospheric forcings can significantly distort the large-scale characteristics of the ocean and sea ice reproduced by ocean-sea ice models and thereby affect the quality of forecasts with such models.

It is worth noting that the above presented results are obtained with the ocean circulation model with a relatively low (~1 deg) horizontal resolution, in which most of the mesoscale oceanic eddies are parametrized. These effects in high-resolution models can be even more pronounced.

**References**

Dussin R., Barnier B., Brodeau L., and Molines J.-M. (2016). The Making of the DRAKKAR Forcing Set DFS5. DRAKKAR/MyOcean Report 01-04-16. 34 p.

Madec G. and the NEMO team (2008). NEMO ocean engine. Note du Pôle de modélisation, Institut Pierre-Simon Laplace (IPSL), France, No 27. ISSN No 1288-1619, 386 pp.

Resnyanskii Yu.D.,and Zelenko A.A. (1999). Effects of Synoptic Variations of Atmospheric Forcing in an Ocean General Circulation Model: Direct and Indirect Manifestations. *Russian Meteorology and Hydrology*. **24**(9), 42–50.

Rousset C., Vancoppenolle M., Madec G. et al. (2015). The Louvain-La-Neuve sea ice model LIM3.6: Global and regional capabilities. *Geosci. Model Dev*., **8**, 2991–3005. https://doi.org/10.5194/gmd-8-2991-2015.